PAPER

Isovalent substitution effects on thermoelectric transport properties of CoSbX (X = S, Se, Te) system

IOP Publishing Journal of Physics: Condensed Matter
J. Phys.: Condens. Matter **31** (2019) 405704 (9pp) https://doi.org/10.1088/1361-648X/ab27b0

Isovalent substitution effects on thermoelectric transport properties of CoSbX (X = S, Se, Te) system

Hafiza Sajida Kousar[1,3], Divya Srivastava[1,2,3], Maarit Karppinen[1] and Girish C Tewari[1,4]

[1] Department of Chemistry and Materials Science, Aalto University, FI-00076 Aalto, Finland
[2] Department of Physics, Central University of Rajasthan, NH-8, Bandar Sindri, Ajmer-305817, Rajasthan, India

E-mail: girish.tewari@aalto.fi

Received 13 March 2019, revised 30 May 2019
Accepted for publication 6 June 2019
Published 15 July 2019

Abstract

We demonstrate a transition of the thermoelectric transport characteristics in the CoSbX (X = S, Se or Te) systems from a *p*-type semiconductor to metallic conductor with increasing size of the X constituent. From DFT calculations CoSbS is found as an indirect semiconductor with band-gap of 0.38 eV, while both CoSbSe and CoSbTe appear as metals. For the two metals, the calculations reveal two degenerate electron pockets (located near the *U* point for CoSbSe and near the *T* point for CoSbTe) and a hole pocket along the *X*-Γ-*Y* points. In line with the theoretical predictions, electrical transport measurements reveal semiconducting-type temperature dependence of resistivity and positive room-temperature Seebeck coefficient (+570 μV K^{-1}) for CoSbS, and metallic-type temperature dependence for CoSbSe and CoSbTe with negative Seebeck coefficient (−14 and −7.5 μV K^{-1}). The Hall coefficient is positive for CoSbS(Se) and negative for CoSbTe. Room-temperature charge carrier densities were estimated at 3×10^{18}/~10^{21}/~10^{22} cm^{-3} for CoSbS/CoSbSe/CoSbTe. Thermal conductivity is dominated by lattice rather than electronic contribution, the RT value being of the roughly same magnitude for all the three compounds. The temperature dependence of thermal conductivity bear resemblance to a typical semiconductor in the case of CoSbS and to a metallic alloy for CoSbSe and CoSbTe.

Keywords: thermoelectric transport, electronic band structure, crystal structure, metal semiconductor transition

(Some figures may appear in colour only in the online journal)

1. Introduction

Thermoelectric (TE) materials possess the ability to convert thermal energy into electrical energy in a reversible fashion. To enhance the conversion efficiency we need to enhance the performance of the TE materials; this is commonly evaluated on the basis of so-called dimensionless figure-of-merit, $ZT = \sigma S^2 T/\kappa$, where σ is electrical conductivity, S is Seebeck coefficient, κ is thermal conductivity and T is absolute temperature. In practice, the initial material performance evaluation is often made based on electrical transport data only, i.e. so-called power factor, PF $= \sigma S^2$.

In recent years, MXY-type compounds have attracted considerable interest as new promising thermoelectric materials. An attractive feature of this family is the flexibility of the structure for chemical substitutions at each of the three sites, which allow multiple ways to tailor the material properties. Indeed, a number of MXY compounds have been synthesized and investigated with the M-site occupied with a 3d transition

[3] Authors contributed equally.
[4] Author to whom any correspondence should be addressed.

metal (Co, Fe, Ni), the X site occupied by a pnictogen (P, As, Sb) and the Y site with a chalcogen (S, Se, Te). The MXY-type compounds typically exist in three interrelated crystallographic structures, i.e. cubic pyrite (space group *Pa*3), orthorhombic marcasite (*Pnn*2/*Pnnm*) and orthorhombic paraarammelsbergite (*Pbca*) [1].

As one of the MXY-type compounds, the natural mineral paracostibite CoSbS [2, 3] has been highlighted as a promising TE material candidate since its discovery from Ontario Red Lake area [4] in Canada; it is a semiconductor with the orthorhombic *Pbca* crystal structure [1, 5, 6]. To further improve its performance, various approaches have been adopted [7–13]. For example, Parker *et al* [7] were able to increase the PF up to ca. 1600 μWK^{-2} m^{-1} through partial Ni-for-Co substitution, but unfortunately with the expense of the higher lattice thermal conductivity. Liu *et al* [8] further challenged the Ni-for-Co substitution in CoSbS and reported a PF value of ca. 2000 μWK^{-2} m^{-1} together with a lower thermal conductivity, i.e. 5.5 WK^{-2} m^{-1} at 300 K. The latter research group attributed the enhanced TE performance to the increased carrier concentration, high effective mass and strong electron-phonon scattering [8].

Recent theoretical predictions of Chmielowski *et al* [9, 10] and You *et al* [12, 13] have suggested that replacing Sb by Te or S by Se could enhance the TE performance of CoSbS. For the Se-for-S replacement, Chmielowski *et al* [9] computed the electronic band structures of CoSbS and CoSbSe in two different space groups. In *Pbca*, both CoSbS and CoSbSe showed semiconducting behavior with indirect band gaps of 0.5 and 0.4 eV, respectively. On the other hand, in $Pnm2_1$ both the compounds manifested semimetallic nature, due to the U pocket of conduction band minimum (CBM) being energetically below the Γ-*Y* pocket of valence band maximum (VBM). Experimentally, for the Se-for-S substituted materials the PF was found to rather decrease, and even though the thermal conductivity also decreased the overall TE performance of CoSbSe remained inferior to the original CoSbS phase. The highest PF values within the Co(Sb,Te)(S,Se) system were achieved when Sb was partially replaced by Te, i.e. ca. 2700 and 1407 μWK^{-2} m^{-1} at 543 and 900 K, respectively.

Another interesting mineral from the MXY class, i.e. cobaltite CoAsS, has been studied by Giese and Kerr [14]. They observed a structural transformation from an orthorhombic structure (with partially disordered anions) to the pyrite structure (*Pa*3) when heated at 800 °C–850 °C; a complete anion ordering was achieved by annealing at 450 °C. Also other MXY-type compounds have been explored for their TE performance, such as CoAsSb [15], NiSbS [7, 16, 17], FeSbS [7], and FeSbTe [18, 19]. Among these, CoAsSb exists in arsenopyrite-type structure ($P2_1/c$) and is an *n*-type semiconductor; the PF was however found to be rather low [15]. On the other hand, NiSbS adopts a cubic crystal structure ($P2_13$) and is metallic; somewhat surprisingly for a metallic phase it showed a relatively high PF value of ca. 1900 μWK^{-2} m^{-1}. Efforts have been made to dope NiSbS with As at the S site and also with Co at the Ni site, but the TE performance has remained moderate so far [17, 20].

Here we chose one of the most promising thermoelectric MXY phases, i.e. CoSbS, for our systematic investigation of isovalent substitution effects from both computational and experimental points of view. Based on our learnings from the previous works, our strategy is to keep the active M site occupied by Co and rather modify our MXY system at the *Y* site. We move within the chalcogen group from S to Se and Te and follow the resultant changes in the crystal and electronic band structures, the type and concentration of carriers and the electrical and thermal transport properties. It should be noted that previous literature mentions only the synthesis of the CoSbSe and CoSbTe compounds, not their transport characteristics (electrical resistivity, Seebeck, thermal conductivity and Hall Effect) [1, 10, 18]. Moreover, by combining both computational and experimental analysis, we are able to gain a comprehensive understanding of the isovalent substitution effects in our CoSb(S/Se/Te) system.

2. Materials and methods

2.1. Sample synthesis

Single-phase samples of the three compounds, CoSbS, CoSbSe and CoSbTe, were prepared from stoichiometric quantities of elemental precursors, i.e. Co powder (99.8%), Sb shots (99.99%), and S, Se or Te shots (99.99%), carefully mixed inside a glove box, pelletized and sealed in quartz ampoules under vacuum for a heat treatment in a tube furnace. For all the three compounds this heat treatment was carried out at 750 °C for 24–48 h, followed by natural cooling to room temperature. However, in the case of CoSbS and CoSbSe, it was mandatory to increase the temperature stepwise to avoid explosion, first to 400 °C in 8 h with a subsequent keeping period of 12 h, then to the target temperature of 750 °C in 6 h. If the temperature is increased continuously the vapour pressure inside the vacuum sealed quartz tube becomes very high and could cause explosion. This happens due to the low boiling temperatures of S (445 °C) and Se (685 °C) in comparison to Te (988 °C). After the first heat treatments the samples were thoroughly homogenized using an agate mortar and pestle in an argon-filled glovebox, then pressed into pellets and sealed again in quartz ampoules for the second sintering at 750 °C.

2.2. Characterization

Each sample was characterized for the phase purity and crystal structure by x-ray diffraction (XRD; PANanalytical X'Pert PRO MPD Alpha-1; Cu Kα1 radiation). The low temperature transport properties (electrical resistivity, Seebeck coefficient, thermal conductivity, Hall coefficient) were measured using a physical property measurement system (PPMS; Quantum design; equipped with 9 T magnetic field). Electrical resistivity, Seebeck coefficient and thermal conductivity were measured simultaneously using the thermal transport option (TTO) available with PPMS. Electrical resistivity and Hall effect were measured by using a standard four-point-probe technique. The thermal conductivity and Seebeck coefficient were measured in isothermal and

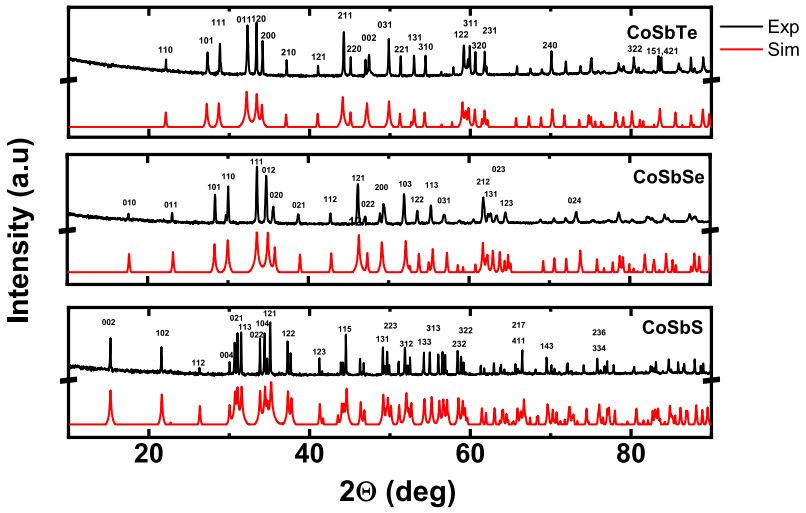

Figure 1. X-ray diffraction patterns for CoSbX (X = S, Se, Te): experimental (black) and simulated (red) based on the DFT-calculated structures. The main peaks are labelled with Miller indices.

open-circuit condition. At a fixed temperature a small amount of heat was applied to one end of a rectangular bar shaped sample. The temperature difference and the Seebeck voltage were measured simultaneously along the length of the sample when the steady state was reached. Seebeck coefficient was estimated by dividing the Seebeck voltage with the temperature difference applied. By using sample dimensions and temperature difference, the thermal conductivity could be obtained.

2.3. Computational details

Density functional theory (DFT) calculations were carried out in GGA framework as implemented in QUANTUM ESPRESSO [21, 22]. The Perdew–Burke–Ernzerhof (PBE) exchange correlation function [23] was used with scalar relativistic PAW pseudopotentials. Spin–orbit coupling (SOC) was not included in the calculations. The plane wave basis cutoff was taken to be 70 Ry. For CoSbSe and CoSbTe, the reducible Brillouin zone was sampled using Monkhorst–Pack type k-point mesh of 21 × 21 × 21 for self-consistent calculations. For CoSbS, the 13 × 13 × 13 k-point grid was used. The lattice constants were obtained by performing the structural optimization until the internal stress was less than 0.2 kbar. In structural optimization, both the atomic positions and lattice constants were free to vary. All the electronic calculations were performed with the optimized lattice constants.

3. Results and discussion

3.1. Structural analysis

All the samples of the three compounds were obtained in single-phase form. In figure 1 we compare the experimental XRD patterns with the corresponding simulated XRD data based on the DFT optimized crystal structures for CoSbS, CoSbSe and CoSbTe (see figure 2); the experimental patterns are indeed in a good agreement with the simulated ones. The

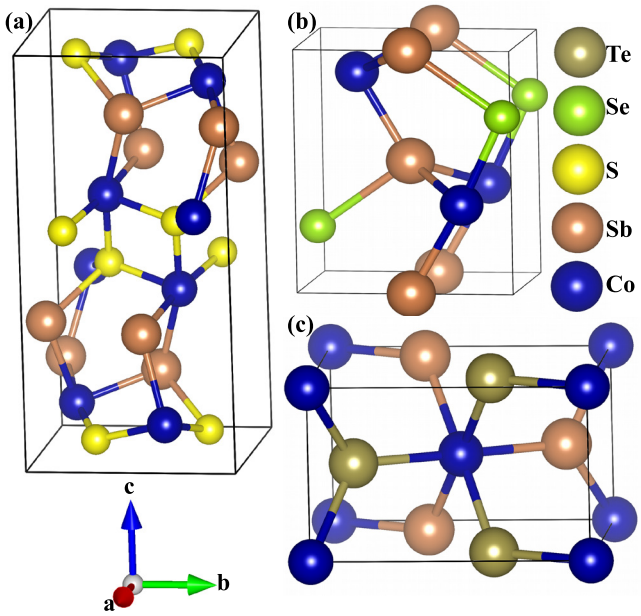

Figure 2. Optimized crystal structures of orthorhombic (a) CoSbS, (b) CoSbSe, and (c) CoSbTe.

CoSbS compound is known to exist in two crystalline forms, paracostibite and costibite, with different numbers of atoms in the unit cell [3–5, 10]. Rietveld refinement confirmed that our CoSbS sample is of the orthorhombic paracostibite structure (*Pbca*; eight formula units per unit cell) [2]; the refined atomic positions and lattice parameters are given in table 1 together with the calculated ones. The XRD pattern for CoSbSe corresponds to orthorhombic structure ($Pnm2_1$; two formula units per unit cell), and the lattice parameters and atomic positions (table 1) are in good agreement with previous published data [10].

The CoSbTe phase has not been studied in detail before, except the preliminary crystal structure parameters reported for the solid-solution $Co(Sb_{1-x}Te_x)_2$ [18]. We refined the structure

Table 1. Experimental and calculated lattice parameters and atomic positions for CoSbX (X = S, Se, Te).

System (space group)		Experimental			DFT		
		x	*y*	*z*	*x*	*y*	*z*
CoSbS (*Pbca*)	Co	0.010(9)	0.164(1)	0.384(2)	0.016	0.167	0.385
	Sb	0.117(9)	0.050(9)	0.180 (1)	0.120	0.049	0.180
	S	−0.134(3)	0.3061)	0.067(3)	−0.134	0.315	0.065
	a; *b*; *c*	5.849 Å; 5.963 Å; 11.682 Å			5.81 Å; 5.94 Å; 11.63 Å		
CoSbSe ($Pnm2_1$)	Co	0.500	0.223(2)	0.869(3)	0.500	0.231	0.866
	Sb	0.500	0.464(2)	0.498(6)	0.500	0.471	0.501
	Se	0.500	0.039(2)	0.231(7)	0.500	0.037	0.230
	a; *b*; *c*	3.690 Å; 5.036 Å; 6.011 Å			3.71 Å; 5.00 Å; 5.97 Å		
CoSbTe (*Pnn*2)	Co	0.000	0.000	0.000	0.001	0.002	0.000
	Sb	0.218(6)	0.359(1)	0.000	0.228	0.359	0.000
	Te	0.218(6)	0.359(1)	0.000	0.782	0.638	0.000
	a; *b*; *c*	5.251 Å; 6.244 Å; 3.834 Å			5.26 Å; 6.23 Å; 3.85 Å		

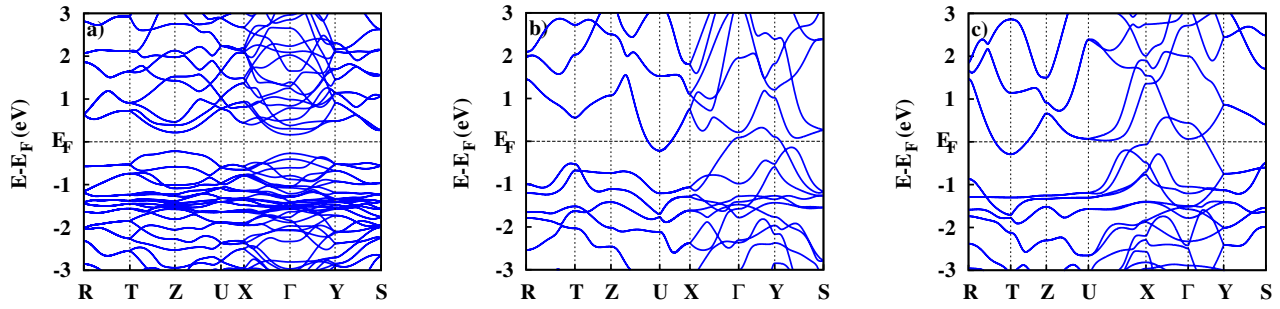

Figure 3. Electronic band structures along high-symmetric points of orthorhombic Brillouin zone for (a) CoSbS, (b) CosbSe, and (c) CoSbTe. Energy zero is set to the Fermi energy.

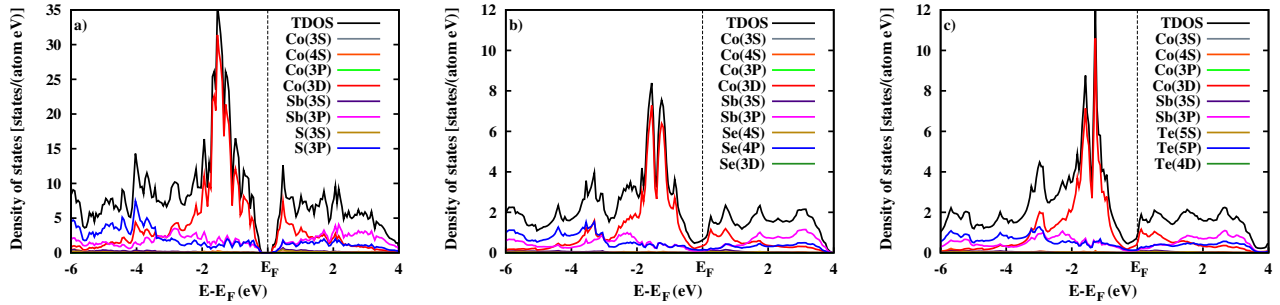

Figure 4. Partial density of states for (a) CoSbS, (b) CosbSe, and (c) CoSbTe. Energy zero is set to the Fermi energy.

of our CoSbTe phase starting from the $NiSb_2$ structure using 'Match' software [3]. The obtained lattice parameters (table 1) are in a good agreement with the data published previously [18]. $NiSb_2$ belongs to the marcasite type structure with orthorhombic phase (*Pnnm*) [4]. However, CoSbTe belongs to space group *Pnn*2 due to absence of mirror reflection, as Co is bonded with two different atomic species in this case, see figure 2(c). From table 1, it can be seen that the DFT calculated lattice constants and atomic positions are in line with experimental value for all the three compounds; the difference in the calculated lattice parameters with respect to experimental values is less than 1% within the conventional GGA.

3.2. Band structures

We display in figure 3 the calculated electronic band structures for the three compounds. In line with the previously reported experimental data, CoSbS is found to be an indirect semiconductor with a band gap of 0.38 eV, while CoSbSe and CoSbTe appear as metallic in our calculations. For CoSbS there are also earlier electronic band structure calculations, showing CoSbS as an indirect band gap semiconductor but with a slightly wider band gap of 0.50 eV [9, 10].

In CoSbS, the Fermi level lies closer to the conduction band, indicating CoSbS to be an *n*-type semiconductor. The valence band edge occurs at *Z* point and the conduction band edge at Γ point. The direct band gaps at *Z* and Γ points are 0.44 and 0.43 eV, respectively. It can be noted from figure 3(a) that both the conduction band (near Γ) and the valence band (near *Z*) are disperse, indicative of heavy effective mass. However, the valence band is flatter than the conduction band. It predicts that the hole effective mass is larger than the electron effective mass.

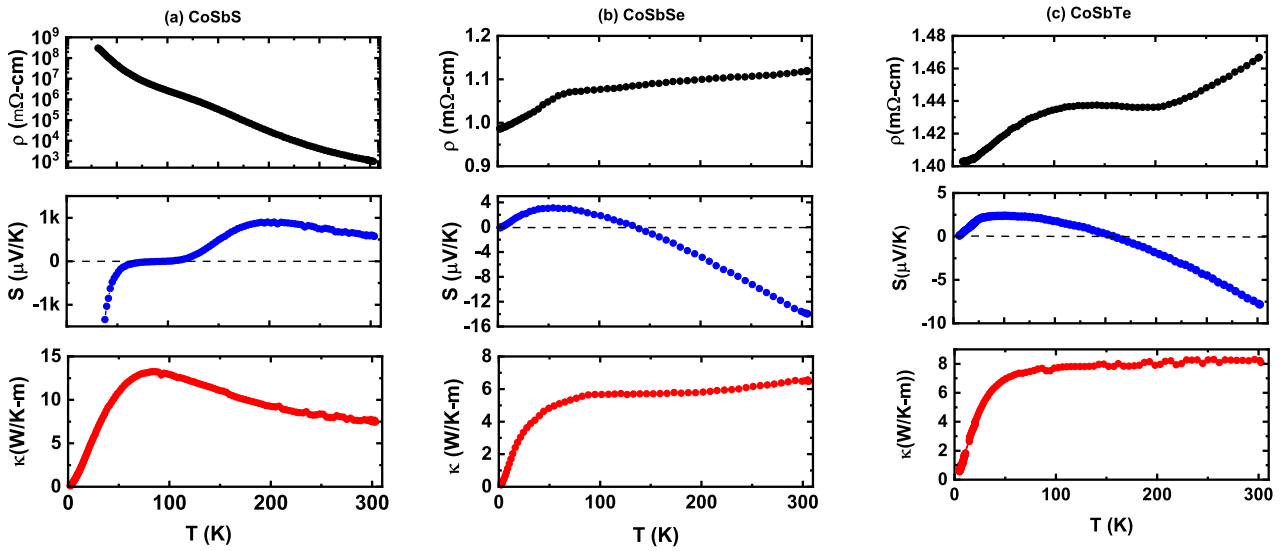

Figure 5. Temperature dependent thermoelectric transport properties of (a) CoSbS (b) CoSbSe, and (c) CoSbTe: electrical resistivity (ρ), Seebeck coefficient (S) and thermal conductivity (κ).

For metallic CoSbSe, three bands are crossing the Fermi level: the doubly degenerate electron-like band near U splits near X and another hole-like along the X-Γ-Y points. The hole pocket is wider than the electron pocket. The overlap between the valence band edge along X-Γ-Y points and the conduction band edge at U point is 0.55 eV. The nonsymmorphic CoSbSe structure may have Weyl band touching point in its electronic structure, see figure 3(b) [24]. In order to see the significant effect of the point, it should be at or very close to the Fermi level. By applying physical or chemical strain one can tune the band structure.

From figure 3(c), the three bands are seen to cross the Fermi level for CoSbTe, creating two electron-like orbits near T and along U-X symmetric points and a hole-like orbit near X-Γ-Y point. The hole pocket is wider than the electron pockets. In CoSbTe, the overlap between the valence and conduction bands is 0.85 eV, i.e. more than that in CoSbSe. There is a band-crossing above E_F along Γ-Y. This system could be topologically interesting along Γ-Y direction.

Figure 4 displays the density of states (DOS) and projected density of states for CoSbS, CoSbSe and CoSbTe. For all the three compounds both the valence band and the conduction band near the Fermi level are dominated by the transition metal d-orbitals which slightly mix with the p-orbitals of the chalcogenide. The sharp increase in DOS at the band edges for CoSbS (figure 4(a)) is in line with our belief that that the valence and conduction bands are heavy mass bands. The heavy mass band explains the large Seebeck coefficient values observed for CoSbS in our experimental evaluation, see figure 5.

The transport properties of CoSbSe and CoSbTe could be significantly enhanced by modifications which would reduce the overlap between the valence and conduction bands. This overlap/band gap depends crucially on structural details, and there are naturally many ways to tune the electronic properties of the materials. For example, pressure could be a powerful tool to tune the electronic and transport properties of these materials. Based on the current results, CoSbSe and CoSbTe with a weak overlap between the edge bands are rather interesting for e.g. topological properties.

3.3. Thermoelectric transport properties

In figure 5, we present the low temperature experimental thermoelectric transport properties measured for the three CoSbX compounds. The upper panel of figure 5 shows the temperature dependence of electrical resistivity (ρ) for these samples. In the case of CoSbS, ρ became very high below 25 K and could not be measured. For CoSbS, a large room-temperature (RT) ρ value of ca. 1.1 Ω cm together with a typical semiconductor behaviour, i.e. increasing ρ with decreasing temperature, are observed, whereas for both CoSbSe and CoSbTe ρ decreases with decreasing temperature, indicating metallic behavior. However, the drop in the ρ values for CoSbSe and CoSbTe on cooling from 300 to 5 K, i.e. 12% and 4%, respectively, is much smaller compared to the cases commonly seen for metals. Moreover, the $\rho(T)$ curve of CoSbTe exhibits a hump below 200 K, and a corresponding transition in the Hall coefficient (R_H) data (lower panel). This could be related to a charge-density-wave transition in these compounds [26], but further studies are definitely needed to affirm this.

The middle panel of figure 5 displays the temperature dependence of Seebeck coefficient data for our CoSbS, CoSbSe and CoSbTe samples. Note that S could not be measured below 25 K due to the high resistance for CoSbS. For CoSbS, the $S(T)$ curve shows large positive S values above 125 K, indicating p-type conduction. Our large RT value of S ($+570$ μV K^{-1}) for CoSbS could be due to the excellent phase purity; also, Liu *et al* [8] have reported an equally high RT S value of $+580$ μV K^{-1}. It is important to note from figure 5 that, at temperatures below ca. 125 K a crossover in the sign of S (from positive to negative) can be seen for CoSbS, indicating that at low temperatures is an n-type conductor in accordance with the present and previous DFT calculation predictions [9]. To the best of our knowledge, thermoelectric properties of CoSbSe and CoSbTe have not been studied before; the only

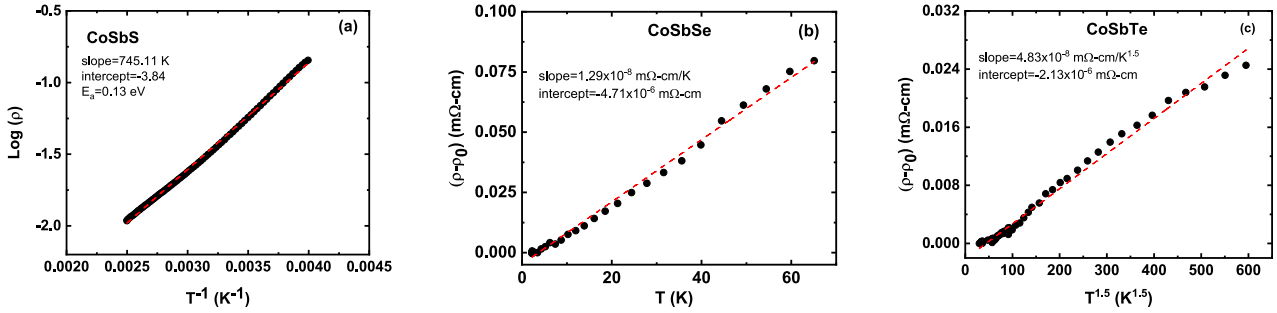

Figure 6. Linear fits (dashed red lines): (a) $\log(\rho)$ versus T^{-1} for CoSbS from 250 to 400 K; activation energy estimated from the linear fit is $E_a = 0.13$ eV. (b) $(\rho - \rho_0)$ versus T for CoSbSe from 5 to 65 K. (c) $(\rho - \rho_0)$ versus $T^{1.5}$ for CoSbTe from 5 to 70 K.

somewhat relevant data are for a 4% Te-doped CoSbSe sample by Chmielowski *et al* [10]. From figure 5, both CoSbSe and CoSbTe show negative S values above 150 K, indicating dominating negative charge carriers (electrons). The RT Seebeck coefficient value is ca. -14 μV K^{-1} for CoSbSe, and slightly lower in magnitude for CoSbTe (-7.5 μV K^{-1}).

Finally, the bottom panel of figure 5 displays the temperature dependence of thermal conductivity (κ) behaviors for our CoSbX samples. It can be seen that for CoSbSe(Te), κ increases sharply with temperature until ca. 70 K, then levels off for the higher temperatures. This behavior looks similar to metallic alloys. The κ is equal to the sum of lattice thermal conductivity (κ_l) and electronic thermal conductivity (κ_e). The κ_l dominates the κ value for all the three compounds. For CoSbSe and CoSbTe, the electronic contribution (κ_e) at RT is ca. 5%–6% and it becomes insignificant at lower temperatures. From figure 5, the κ for CoSbS—after the rapid increase at low temperatures—passes through a maximum around 90 K and then decreases at the higher temperatures approximately following the $1/T$ behavior, which is the signature of phonon scattering [7]. The κ_e for CoSbS is negligible in whole temperature range, which is consistent with the $1/T$ behavior expected for the lattice term.

We carried out further analysis of the experimental results for the deeper insights into the transport phenomena in the CoSbX system. The first member, CoSbS is a semiconductor and to estimate the band gap energy (E_g) or activation energy (E_a), we plot $\log(\rho)$ versus T^{-1} from 250 to 400 K in figure 6(a). The linear fit yields, $E_a = 0.13$ eV, which is lower than E_g of 0.38 eV, predicted by the electronic band structure calculations. The deviation suggests a doped semiconductor. The doping might be related to interstitial defects and disorder created during synthesis of the current sample. The other two members, CoSbSe and CoSbTe showed metallic behavior. At low temperatures below 65 K, ρ for CoSbSe showed a linear T dependence, see figure 6(b) where we plot $(\rho - \rho_0)$ versus T from 5 to 65 K, ρ_0 is residual resistivity. For CoSbTe, on the other hand, ρ approximately follows $T^{1.5}$ rather than T at low temperatures (5–70 K), see figure 6(c). Notably, the T or $T^{1.5}$ dependence of ρ as seen for CoSbSe and CoSbTe is indicative of a non-Fermi-liquid (NFL) like behavior [26–28]. In conventional metals electron–electron and electron-phonon scattering dominates the conduction. At low T the electron–electron scattering takes over conduction and gives rise to a T^2 dependence of ρ. The T or $T^{1.5}$ dependence of ρ upto fairly high temperature of 65 K in the present metallic compounds suggest that the conduction cannot be explained by conventional scattering processes. A similar behavior of ρ in a wide T range has been observed in the normal state of Sr-doped $LaCuO_4$ and $YBa_2Cu_3O_7$ superconductors, where the behavior can be attributed to weak electron-phonon coupling [26, 27].

At low T, S for metals can be written as $S = S_d + S_g = AT + BT^3$, where A, B are constants, S_d is diffusion term and S_g is phonon drag term [29]. This equation is valid in the temperature region $T \ll \theta_D$, where θ_D is Debye temperature. To estimate the S_g for CoSbSe(Te), we plot S/T versus T^2 from 5 to 25 K in figure 7(a). From $S/T = A + BT^2$, and the slope of S/T versus T^2 the value of B is obtained, and the intercept gives the value of A. The S/T versus T^2 plot for CoSbSe(Te) does not show linear behavior; rather the S in the CoSbSe(Te) systems depends linearly on T from 5 to 25 K with approximately the same slope, see figure 7(b). The linear fits at low temperatures for CoSbSe and CoSbTe indicate that the S_d dominates the S in these compounds at least up to 25 K. The T or $T^{1.5}$ dependence of ρ, which is related to weak electron-phonon coupling also supports this behavior of small S_g [26, 27]. At high T, near the crossover region, the S_g might contribute significantly. The estimation of S_g in this region is more demanding due to complicated T dependence of S_d.

We also measured the temperature-dependence of Hall coefficient (R_H) and estimated the carrier concentrations (n) for all the studied compounds, see figure 8. At a fixed temperature the Hall voltage (V_H) was measured by applying a constant direct current (DC) and sweeping the magnetic field from -8 T to $+8$ T. The R_H was estimated from the slope of this curve, $V_H = R_H\left(\frac{I \times B}{t}\right)$, where I is applied current, B is magnetic field and t is thickness of sample. In case of CoSbS, the Hall voltage could not be measured below 120 K due to high resistance. For CoSbS and CoSbSe, R_H is positive in the entire temperature range see figures 8(a) and (b), and the RT value of $n \approx 10^{18}$ cm^{-3}, 10^{21} cm^{-3} is typical for a semiconductor and a metal respectively. Most of the previous studies have presented CoSbS as an n-type semiconductor [7–10]. However, our positive R_H value above 120 K and the positive S value at temperatures above ca. 125 K, both indicating that CoSbS (in paracostibite phase) is a p-type semiconductor at high temperatures. From figure 8(a), R_H decreases nearly exponentially with temperature for CoSbS, and n increases about five order of magnitude in the same temperature range; R_H and n are inversely related to each other ($R_H = 1/ne$), where e is electronic charge.

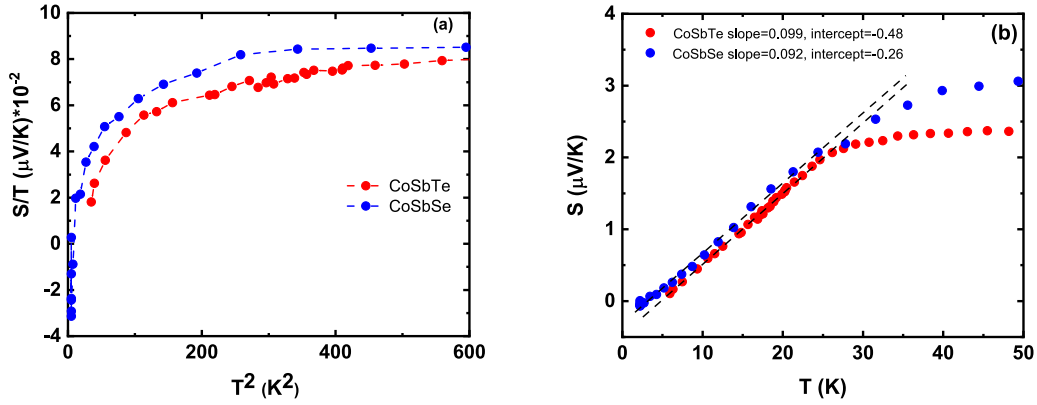

Figure 7. (a) S/T versus T^2 for CoSbSe(Te) at low temperature from 5 K to 25 K. (b) Linear fit (dashed red lines) S versus T for CoSbSe and CoSbTe from 5 to 25 K.

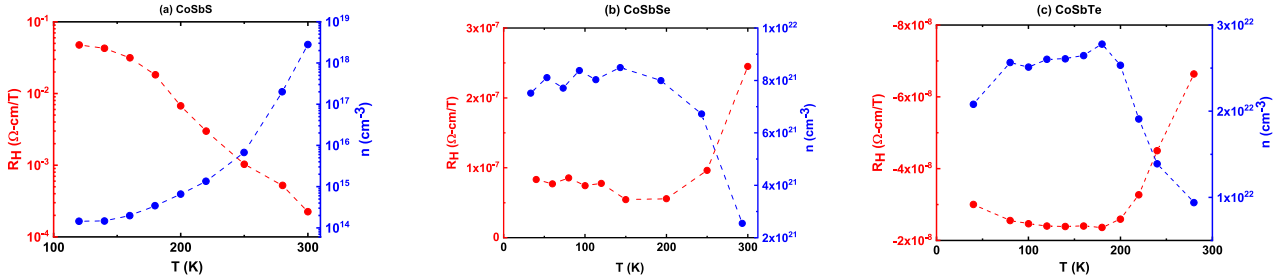

Figure 8. T dependent R_H and n for (a) CoSbS, (b) CoSbSe and (c) CoSbTe. Note that R_H was found to be positive for CoSbS, CoSbSe and negative for CoSbTe throughout the T range measured.

For CoSbTe, R_H is negative thorough the temperature range measured in accordance with the electronic transport being dominated by electrons. The n value is in the range of 10^{22} cm^{-3}, being thus consistent with the metallic nature of CoSbTe. For both CoSbSe and CoSbTe, with increasing temperature, n first slightly increases and then remains nearly constant up to 200 K, followed by a sharp decrease at the higher temperatures; the R_H value shows a similar but inverse behavior with increasing temperature. It should be noted that this behavior resembles the $\rho(T)$ curve and could be explained by a charge-density-wave type transition [25] as we already mentioned earlier. The S show a crossover (see figure 5) from positive to negative for CoSbS and negative to positive for CoSbSe(Te) systems with decreasing T. The R_H however, does not show a change of sign around that T. It remained positive for CoSbS(Se) and negative for CoSbTe. Many conventional metals like Cu, Ag, Au [30] and Li [31] show the sign of S opposite to that of the R_H. This contrasting behavior of S and R_H is related to the Fermi surface [32]. The spherical Fermi surface consists of necks and Bellies at the Brillouin zone and the positive and negative curvature near the neck and belly generates hole-like and electron-like states at the Fermi surface. The density of hole-like states is larger than the density of electron-like states, which results in positive Seebeck coefficient in these metals. In case of currently studied CoSbSe(Te) systems, the opposite signs of S compare to R_H might be explained by similar phenomenon. The electronic band structures presented in figure 3 also showed contribution from both electron and hole pockets near the Fermi level.

4. Discussion and conclusions

We have used a combined experimental and theoretical approach to systematically investigate the thermoelectric transport properties in the CoSb(S/Se/Te) system. The CoSbS member of this system was known as one of the most promising thermoelectric MXY-type phases, but very little was known of the other two members, i.e. CoSbSe and CoSbTe. In general, isovalent substitution or so-called chemical pressure has been a highly successful means to tailor the properties of thermoelectric materials. In this work our strategy was to keep the active Co site in CoSbS untouched and modify the structure at the chalcogenide site.

We followed the changes in the crystal and electronic band structures, the type and concentration of carriers and the electrical and thermal transport properties upon replacing sulfur with its Periodic Table group members, selenium and tellurium, and using a comprehensive set of experimental and computational techniques for the characterization. All the three compounds crystallize in orthorhombic structure but with different crystal symmetries, the space group changing from *Pbca* for CoSbS to $Pnm2_1$ for CoSbSe and *Pnn*2 for CoSbTe. Electronic band structure calculations revealed CoSbS as an indirect band gap semiconductor (band gap ~0.38 eV) and CoSbSe and CoSbTe as metallic.

Our experimentally observed transport property results were perfectly in line with the theoretical results. The temperature dependence of electrical resistivity and charge carrier density affirmed the semiconductor to metal transition, when S was replaced with Se or Te, accompanied with a

significant reduction in the absolute value of Seebeck coefficient. The main contribution at the Fermi level comes from Co 3*d*-orbitals and Se or Te 4*p*-orbitals. The overlap gives rise to mixed charge carriers (electrons and holes) and enhance the carrier concentrations in CoSbSe and CoSbTe. This may be the reason for the small Seebeck coefficients in these two metallic compounds.

Apart from the aforementioned observations, we also saw a sign change in the temperature dependence of Seebeck coefficient for the CoSb(S/Se/Te) systems. However, the R_H does not show a sign change. In case of CoSbSe(Te), the opposite signs of S in comparison to R_H might be related to the electronic band structure at Fermi level. In CoSbS, both the conduction bands and the valance bands are flat near Fermi level and can cause high effective masses for electrons and holes. The effective mass is inversely proportional to the first derivative of the band. The large p-type Seebeck coefficient in CoSbS might be related to high effective mass of the charge carriers. In the CoSb(S/Se/Te) system, the absolute value of Seebeck coefficient decreases significantly on the substitution of S with Se or Te. This is due to the increase in density of states near the Fermi level as going from CoSbS to CoSbTe. Finally, we demonstrated that thermal conductivity of these compounds is dominated by phonon conductivity. It could thus be reduced by introducing e.g. disorder, defects, or doping.

Acknowledgments

The present work has received funding from the Academy of Finland (Nos. 292431 and 303452). This work also made use of the RawMatTERS Finland infrastructure (RAMI) facilities based at Aalto University. DS would like acknowledge DST, India for INSPIRE faculty award (No. DST/INSPIRE/04/2015/000579) and CSC—the Finnish IT Center for Science for computational resources.

ORCID iDs

Maarit Karppinen https://orcid.org/0000-0003-1091-1169
Girish C Tewari https://orcid.org/0000-0002-0350-5165

References

[1] Henry R, Steger J, Nahigian H and Wold A 1975 High pressure synthesis and properties of coxy compounds (X = phosphorus, arsenic, antimony, and Y = sulfur, selenium) *Inorg. Chem.* **14** 2915–7
[2] Rowland J F, Gabe E J and Hall S R 1975 The crystal structures of costibite (CoSbS) and paracostibite (CoSbS) *Can. Mineral.* **13** 188–96
[3] Zakrzewski M A, Burke E A J and Nugteren H W 1980 Cobalt minerals in the Hallefors Area, Bergslagen, Sweden: new occurrences Of costibite, paracostibite, nisbite and cobaltian ullmannite *Can. Mineral.* **18** 165–71
[4] Cabri L J, Harris D C and Stewart J M 1970 Paracostibite (CoSbS) and nisbite (NiSb2), new minerals from the red lake area, Ontario, Canada *Can. Mineral.* **10** 232–46
[5] Cabri L J, Harris D C and Stewart J M 1970 Costibite (CoSbS), a new mineral from Broken Hill, N.S.W., Australia *Am. Mineral.* **55** 10–17
[6] Nahigian H, Steger J, McKinzie H L, Arnott R J and Wold A 1974 Preparation and characterization of some cobalt phosphorus, cobalt arsenic, cobalt antimony sulfide or selenide compounds *Inorg. Chem.* **13** 1498–503
[7] Parker D, May A F, Wang H, McGuire M A, Sales B C and Singh D J 2013 Electronic and thermoelectric properties of CoSbS and FeSbS *Phys. Rev.* B **87** 045205
[8] Liu Z, Geng H, Shuai J, Wang Z, Mao J, Wang D, Jie Q, Cai W, Sui J and Ren Z 2015 The effect of nickel doping on electron and phonon transport in the n-type nanostructured thermoelectric material CoSbS *J. Mater. Chem.* C **3** 10442–50
[9] Chmielowski R, Bhattacharya S, Jacob S, Péré D, Jacob A, Moriya K, Delatouche B, Roussel P, Madsen G and Dennler G 2017 Strong reduction of thermal conductivity and enhanced thermoelectric properties in $CoSbS_{1-x}Se_x$ paracostibite *Sci. Rep.* **7** 46630
[10] Chmielowski R, Bhattacharya S, Xie W, Péré D, Jacob S, Stern R, Moriya K, Weidenkaff A, Madsen G K H and Dennler G 2016 High thermoelectric performance of tellurium doped paracostibite *J. Mater. Chem.* C **4** 3094–100
[11] Kaur P and Bera C 2017 Effect of alloying on thermal conductivity and thermoelectric properties of CoAsS and CoSbS *Phys. Chem. Chem. Phys.* **19** 24928–33
[12] You Y, Su X, Liu W, Yan Y, Hu T, Uher C and Tang X 2017 Modification of the intermediate band and thermoelectric properties in Se-doped $CoSbS_{1-x}Se_x$ compounds *RSC Adv.* **7** 34466–72
[13] You Y, Su X, Liu W, Yan Y, Fu J, Cheng X, Zhang C and Tang X 2018 Structure and thermoelectric property of Te doped paracostibite $CoSb_{1-x}Te_xS$ compounds *J. Solid State Chem.* **262** 1–7
[14] Giese R F Jr and Kerr P F 1965 The crystal structures of ordered and disordered Cobaltite *Am. Mineral.* **50** 1002–14
[15] Tan X *et al* 2018 Thermoelectric properties of CoAsSb: An experimental and theoretical study *Chem. Mater.* **30** 4207–15
[16] Carlini R, Zanicchi G, Borzone G, Parodi N and Costa G A 2012 Synthesis and characterization of the intermetallic compound NiSbS *J. Therm. Anal. Calorim.* **108** 793–7
[17] Miyata M, Ozaki T, Nishino S and Koyano M 2017 Thermoelectric properties of high power factor sulfide NiSbS and Co substitution system $Ni_{1-x}Co_xSbS$ *Japan. J. Appl. Phys.* **56** 021801
[18] Yamaguchi G, Shimada M and Koizumi M 1976 Preparation and crystal structure of $Fe(Sb_{1-x}Te_x)_2$ and $Co(Sb_{1-x}Te_x)_2$ $(0 \leq x \leq 1)$ *J. Solid State Chem.* **19** 63–5
[19] Yamaguchi G, Shimada M, Koizumi M and Kanamaru F 1980 Preparation and characterization of compounds of the system $Fe(Sb_{1-x}Te_x)_2$ $(0 \leq x \leq 1)$ *J. Solid State Chem.* **34** 241–5
[20] Carlini R, Macciò D, Pani M, Parodi N, Zanicchi G, Carnasciali M M and Costa G A 2013 Synthesis and thermal properties of NiSbS–As doped phase *J. Therm. Anal. Calorim.* **112** 513–7

[21] Giannozzi P *et al* 2017 Advanced capabilities for materials modelling with quantum ESPRESSO *J. Phys.: Condens. Matter* **29** 465901
[22] Wentzcovitch P G *et al* 2009 Quantum ESPRESSO: a modular and open-source software project for quantum simulations of materials *J. Phys.: Condens. Matter* **21** 395502
[23] Perdew J P, Burke K and Ernzerhof M 1996 Generalized gradient approximation made simple *Phys. Rev. Lett.* **77** 3865–8
[24] Furusaki A 2017 Weyl points and Dirac lines protected by multiple screw rotations *Sci. Bull.* **62** 788–94
[25] Zhai H-F *et al* 2014 Possible charge-density wave, superconductivity, and f -electron valence instability in $EuBiS_2F$ *Phys. Rev.* B **90** 64518
[26] Gurvitch M and Fiory A T 1987 Resistivity of $La_{1.825}Sr_{0.175}CuO_4$ and $YBa_2Cu_3O_7$ to 1100 K: absence of saturation and its implications *Phys. Rev. Lett.* **59** 1337–40
[27] Takagi H, Batlogg B, Kao H L, Kwo J, Cava R J, Krajewski J J and Peck W F 1992 Systematic evolution of temperature-dependent resistivity in $La_{2-x}Sr_xCuO_4$ *Phys. Rev. Lett.* **69** 2975–8
[28] Belitz D and Kirkpatrick T R 2018 Anomalous transport behavior in quantum magnets *Condens. Matter* **3** 30
[29] Blatt F J, Schroeder P A, Foiles C L and Greig D *1976* The thermoelectric power of transition metals *Thermoelectric Power of Metals* (Boston, MA: Springer)
[30] Hurd Colin M 1972 *The Hall Effect in Metals and Alloys* (New York: Plenum Press)
[31] Xu B and Verstraete M J 2014 First principles explanation of the positive seebeck coefficient of lithium *Phys. Rev. Lett.* **112** 196603
[32] Fujita S, Ho H-C and Okamura Y 2000 Quantum theory of the Seebeck coefficient in metals *Int. J. Mod. Phys.* B **14** 2231–40